Chapter 15
Stress Analysis on Welded Specimen with Multiple Methods

Sanichiro Yoshida, Tomohiro Sasaki, Sean Craft, Masaru Usui, Jeremy Haase, Tyler Becker, and Ik-Keun Park

Abstract Effects of the thermal stress due to welding on the mechanical property of the welded work are analyzed with multiple methods. Strain gauges and an acoustic microscope are used to measure the residual stress, and electronic speckle pattern interferometry (ESPI) is used to analyze the response of the welded wok to external force. A tensile load is applied to butt-welded, thin-plate steel specimens, and the resultant strain field is analyzed with the ESPI. Comparison is made with the case of a non-welded specimen of the same material and dimensions. The analyses indicate that the residual stress due to welding makes the normal strain due to the external tensile load asymmetric. The asymmetry enhances shear and rotational modes of deformation, generating stress concentration at a point away from the weld where the residual stress is substantially negligible.

Keywords Residual stress • Electronic speckle-pattern interferometry • Acoustoelasticity • Welding • Strain analysis

15.1 Introduction

The stress field near a weld is complicated. Thermal load during the weld generates a permanent stress locked in the material. This type of stress is known as the residual stress and is harmful to the welded work as it accelerates deformation and even leads to a failure of the work. The mechanism of residual stress is generally explained as follows. During the heating phase, thermally expanded regions stretch the surrounding material. Consequently, the surrounding regions experience tensile stress. During the cooling phase, the previously expanded regions get stretched as they shrink whereas the surrounding regions get compressively stressed (because the surrounding area does not shrink). Thus, the welded work tends to have tensile residual stresses near the weld and compressive residual stresses in the other regions. However, in reality, the pattern of residuals stress is not as simple as this. It depends on various factors such as the shape of the work, the thermal conductivity of the material and the welding conditions.

A number of theoretical and experimental studies are reported on residual stresses due to welding [1–3]. These studies mostly focus on the analysis, removal or prevention of the residual stresses. As a stress hidden in the material, detection of residual stress is quite challenging and these types of studies are extremely important. What is also important, however, is to understand the response of materials with residual stresses when an external force is applied. It is most likely that the welded work is used under the influence of a certain external force; as an example, the stress due to the inner pressure on the welded-wall of a high-pressure vessel. It should be noted that simple superposition of residual stresses and the stress due to an external load at the point of residually stressed area is not sufficient to understand the behavior of the welded work. Normally, the action point of the external load is distanced from the point of residual stress. When the external force acts on

S. Yoshida (✉) • S. Craft • J. Haase • T. Becker
Department of Chemistry and Physics, Southeastern Louisiana University, SLU 10878, Hammond, LA 70402, USA
e-mail: syoshida@selu.edu; sanichiro.yoshida@selu.edu

T. Sasaki • M. Usui
Department of Mechanical Engineering, Niigata University, IkarashinNinocho 8050, Nishi-ku, Niigata-shi, Niigata 950-2181, Japan

I.-K. Park
Department of Mechanical and Aotomotive Engineering, Seoul National University of Science and Technology,
232 Gongneung-ro, Nowon-gu, Seoul 139-743, South Korea

H. Jin et al. (eds.), *Advancement of Optical Methods in Experimental Mechanics, Volume 3: Proceedings of the 2014 Annual Conference on Experimental and Applied Mechanics*, Conference Proceedings of the Society for Experimental Mechanics Series, DOI 10.1007/978-3-319-06986-9_15,

the work, the force is transferred from the action point to the entire work in accordance with the elastic property of each point. Residual stresses alter the local elastic constant of the material; as widely known, a compressive stress due to the thermal load from a welding torch can easily cause permanent plastic strain. Therefore, the response to the external force of the entire work containing residual stresses is substantially different from that without residual stresses.

The aim of this study is to explore this exact question of "how do the residual stresses alter the response of welded work to external force?" To this end, a low-level tensile load is applied to a butt-welded thin-plate specimen and its response is compared with the response of a non-welded specimen of the same dimension and material. An electronic speckle pattern interferometer (ESPI) is used to analyze the specimen's behavior as a full-field image. A strain gauges and a scanning acoustic microscope are used to analyze the residual stress. The results indicate that the change in the elastic constant due to the residual stress near the weld alters the pattern of overall deformation, making it less symmetric around the central line of the specimen (both parallel and perpendicular to the tensile axis). This generates strain concentration at a point away from the weld line, causing more bodily rotation in response to the applied tensile load.

15.2 Experimental

The materials tested in this study were cold-rolled carbon steel plates. Two types of welded specimens were prepared. For the first type (specimen 1), two plates of 90 mm (wide) × 50 mm (long) × 0.4 mm (thick) were butt-welded into a plate of 90 mm × 100 mm × 0.4 mm, and cut into 20 mm wide × 100 mm long specimens (Fig. 15.1a). The second type (specimen 2) was prepared in a similar fashion but the final dimension was 40 mm wide × 150 mm long × 3 mm thick (Fig. 15.1b). For each type, a non-welded specimen of the same dimension was prepared as the control.

The specimen was attached to a tensile machine for application of a tensile load. An ESPI setup sensitive to in-plane displacement was arranged in front of the tensile machine (Fig. 15.2). Fringe patterns were formed by subtracting the image taken before the application of the tensile load from the image taken after the application of the load. The phase associated with the displacement was evaluated by assigning the order to each fringe and interpolating the phase between fringes. A care was taken to apply as small load as possible to avoid plastic deformation caused by the tensile load. For comparison, a non-welded specimen of the same material and dimension was tested in the same fashion.

A challenge in the application of the ESPI as stated above to analysis of residual stresses due to welding is that the phase analysis on the formed fringes is not easy. Often the welded specimen exhibits bodily rotation, which yields fringes parallel to the sensitivity vector of the ESPI interferometer. When the interferometer is sensitive to horizontal displacement, for example, the fringe pattern is approximately equidistant, horizontally parallel, as Fig. 15.3a indicates. This makes difficult to evaluate the normal strain, because the variation of the fringe order along the axis is small (in the case of Fig. 15.3a, the change in the fringe order in going horizontally from the left end of the image to the right end is two or less). As a solution to this issue, a system of carrier fringes was introduced by rotating the wedge placed after the beam expander for the left interferometric arm. The wedge was rotated after the tensile load was applied. The rotation of the wedge provided a constant phase variation along the tensile axis on the specimen as Fig. 15.2b indicates. The provision of the carrier fringe altered the fringe pattern from Fig. 15.3a to Fig. 15.3c. Now that the horizontal variation in the fringe order was high, the phase could be

Fig. 15.1 Butt-welded specimen 1 (**a**) and specimen 2 (**b**). The *box with dashed lines* indicates approximate area of view. For specimen 2 strain was measured with strain gauges at 12 points; 5 mm and 20 mm away from the weld line along the tensile axis, 16 mm above/below the central line parallel to the tensile axis. *Circles* indicate these locations for the *right side* of the weld line only. Strain gauge measurements were made on the *left side* of the weld line at the locations symmetric to these six points. The circle and distances inserted in (**a**) indicate the locations where acoustic velocity is previously measured in a welded specimen similar to this study

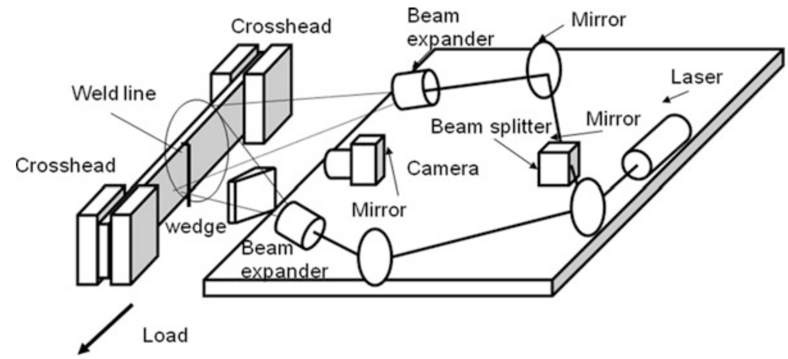

Fig. 15.2 Experimental arrangement. The optical wedge is to introduce carrier fringes

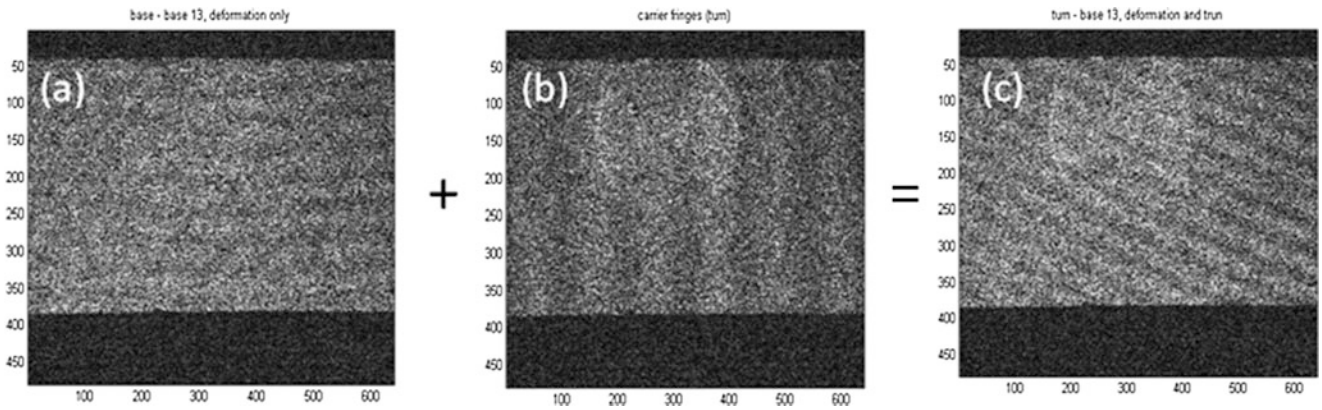

Fig. 15.3 Typical fringe patterns. (**a**) deformation only; (**b**) carrier fringes; (**c**) deformation plus carrier fringes

evaluated with a reasonable accuracy by interpolation. The true phase change was evaluated by subtracting the known phase change due to the wedge rotation (Fig. 15.3b) from the total phase variation (Fig. 15.3c).

For specimen 2, residual strain was measured with a strain gauge. After the tensile experiment was completed, the specimen was detached from the tensile machine, and a pair of strain gauges oriented along the tensile axis and perpendicular to it was attached at 12 reference points near the weld as indicated in Fig. 15.1b. After strain was measured at each point for both x and y directions, these points were isolated by cutting as a square of approximately 9 mm $\times$ 9 mm around the point. After the isolation, the strains were measured again. The difference of the strain gauge reading before and after the isolation was interpreted as the residual strain. Each measurement was repeated five times and the average of the five measurements was employed.

15.3 Results and Discussion

Table 15.1 summarizes the tensile experiments conducted for the two types of specimens. The same load was applied to the non-welded and welded specimens. "Average strain" is calculated from the displacement of the tensile machine's crosshead and the gauge length of the specimen (the former divided by the latter). The average stress is calculated from the tensile machine's load reading (the difference between the load cell reading when the fist ESPI image is taken and that when the second ESPI image is taken). The maximum stress (x) and (y) are evaluated from the maximum values of the strain gauge's reading at the 12 measurement points (Fig. 15.1b).

Figure 15.4 are normal strain (ε_{yy}) along the tensile axis (y) obtained from the fringe analysis on specimen 1 for the non-welded (left) and welded (right) case. The box drawn near the center of the y-axis indicates the location of the weld. The strain levels are close to the average strains shown in Table 15.1.

Comparison of the non-welded and welded cases in Fig. 15.4 indicates the following features. Generally, the strain of the non-welded specimen is much smoother than that of the welded specimen. The strain field of the welded specimen appears more or less symmetric along the y-axis (parallel to the tensile axis) about the weld line. It appears that the normal strain vigorously fluctuates along the x-axis (perpendicular to the tensile axis) than y-axis over the all region, not necessarily near

Table 15.1 Summary of tensile experiment on Specimen 1 and 2

	Specimen 1		Specimen 2			
	Average strain (cross head reading)	Average stress (load cell) (MPa)	Average strain (cross head reading)	Average stress (load cell) (MPa)	Max stress (y) (strain gauge) (MPa)	Max stress (x) (strain gauge) (MPa)
Non-welded	1.00×10^{-4}	1.25	6.29×10^{-4}	15.9	–	–
Welded	2.00×10^{-4}	1.25	6.29×10^{-4}	17.2	168.7	−224.96

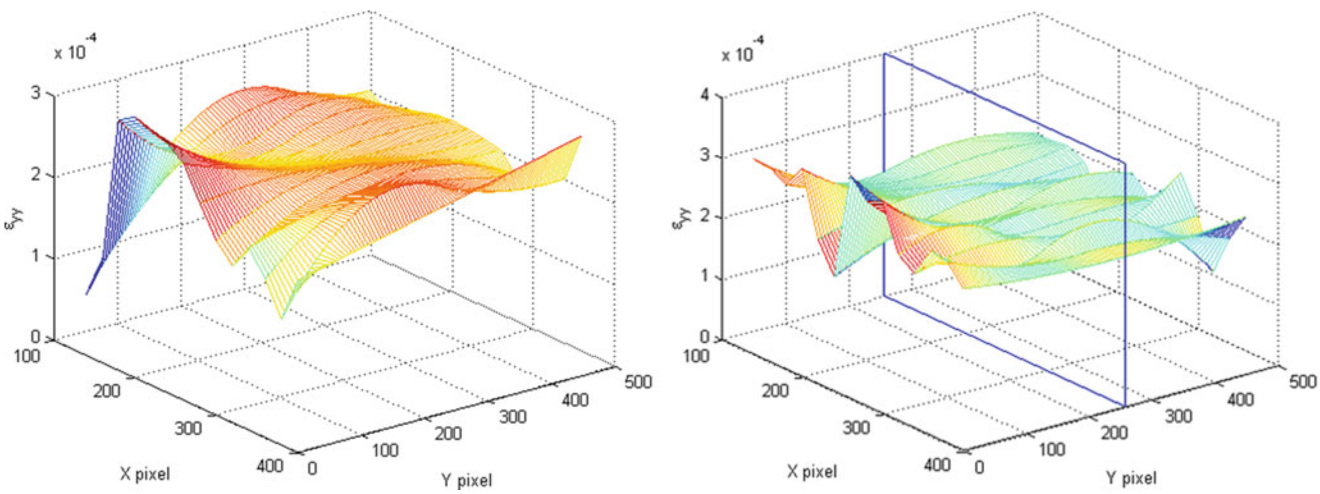

Fig. 15.4 Normal strain observed in non-welded (*left*) and welded (*right*) specimen 1

the weld line. This is explained by considering that the residual stress due to welding is mainly caused by the cooling and heating effects of the welding laser beam as it sweeps along the weld line. It is consistent with Karlsson's observation [3] that the residual stress due to weld is greater parallel to the weld than perpendicular to it. The high spatial frequency in the fluctuation of the strain along the x-axis indicates that the heating and cooling effect associated with the passage of the welding laser beam is rather fast. This spatial frequency may depend on the speed of the welding, which is an interesting subject for future study. The strain fluctuations along the x- and y-axis, i.e. parallel and perpendicular to the weld line, are more explicitly analyzed in Figs. 15.5 and 15.6 where the strain of the welded specimen is compared with that of the non-welded specimen for several lines perpendicular and parallel to the weld line.

It is well known that the elastic constant of materials changes under stress. The reason for the change is that a stress alters the inter-atomic distance and that the inter-atomic potential is not symmetric except the vicinity of the equilibrium. In most materials, the inter-atomic potential is steeper on the short-distance side of the equilibrium than the long-distance side, whereas it is approximately a quadratic function of the inter-atomic distance near the equilibrium. Acoustoelasticity utilizes this fact [4–6]. When an elastic medium is under a compressive stress, the inter-atomic distance is decreased and therefore the elastic constant, the change in the slope of the inter-atomic potential, becomes higher than around the equilibrium. On the contrary, when an elastic medium is under a tensile stress, the elastic constant becomes lower than the equilibrium. Consequently, the acoustic phase-velocity, which is proportional to the square root of the elastic constant, increases/decreases under a compressive/tensile stress. A previous study (C. Miyasaka, private communication, 2013) shows that the acoustic velocity varies ±6 % along a line parallel to the weld line in a SPCC specimen similar to this study, as shown in Fig. 15.7. Here the horizontal axis indicates the distance from the center of the specimen along a line parallel to the weld line and 3 mm away from it. The same study indicates that the acoustic velocity measured at 7 mm away from the weld line is not affected by the welding. The points of measurement are indicated in Fig. 15.1a.

Although the non-welded and welded data are based on two independent ESPI measurements, the applied tensile load is identical. Therefore, the strain data of the non-welded and welded specimen shown in Fig. 15.4 are proportional to the compliance, and a comparison between the two cases should indicate the relative compliance reflecting the effect of welding. Figure 15.8 plots the strain data of the welded specimen divided by that of the non-welded specimen (the relative compliance plot). Also plotted in this figure is the maximum and minimum relative compliance calculated from the 6 % variation of the acoustic velocity data shown in Fig. 15.7. It is seen that the relative compliance plot fits between the maximum and minimum

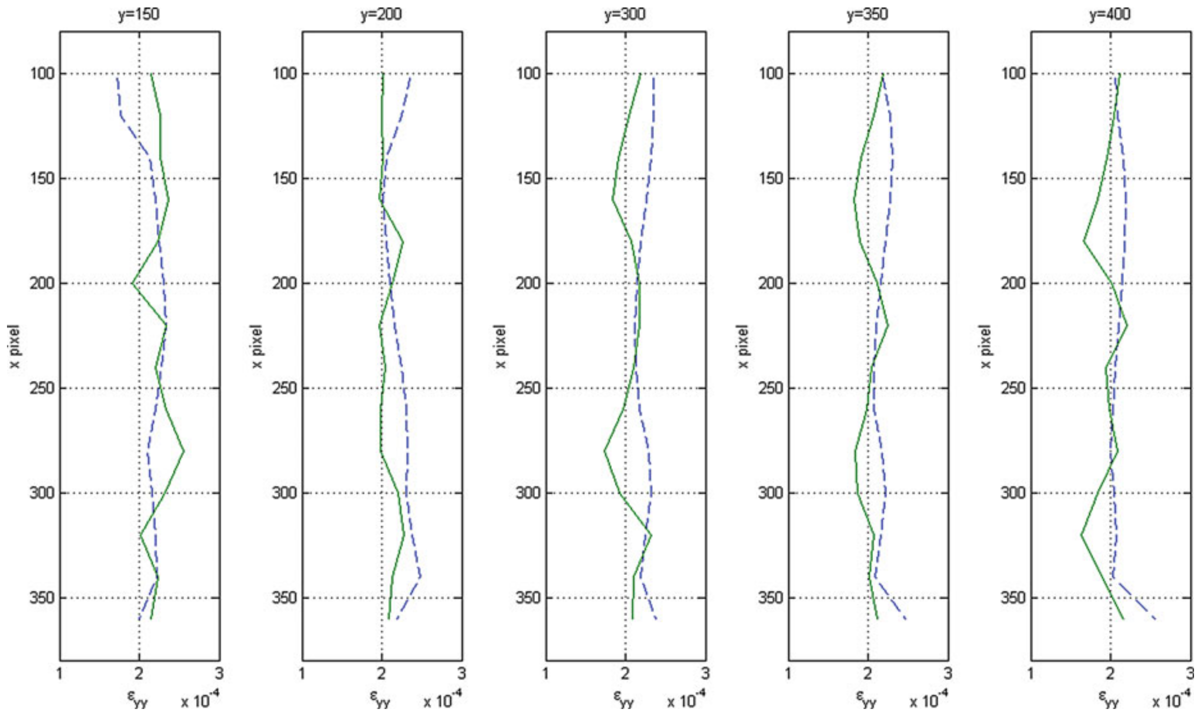

Fig. 15.5 Dependence of ε_{yy} on x (parallel to weld line). The solid line is for the welded specimen and the dashed line is for the non-welded specimen

Fig. 15.6 Dependence of ε_{yy} on y (perpendicular to weld line). The solid line is for the welded specimen and the dashed line is for the non-welded specimen

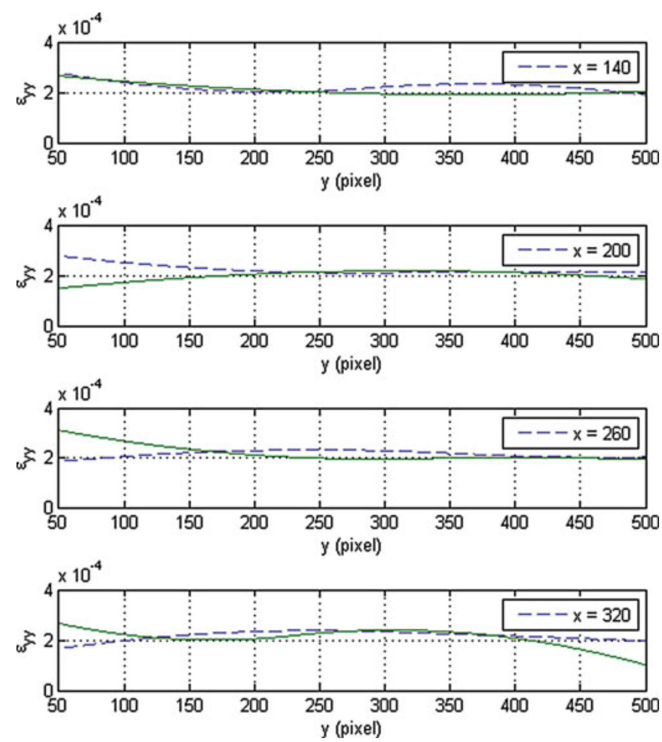

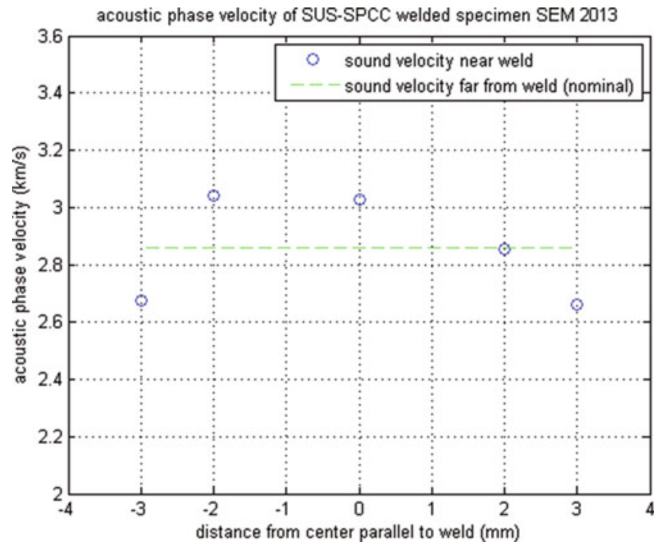

Fig. 15.7 Acoustic velocity measured near weld

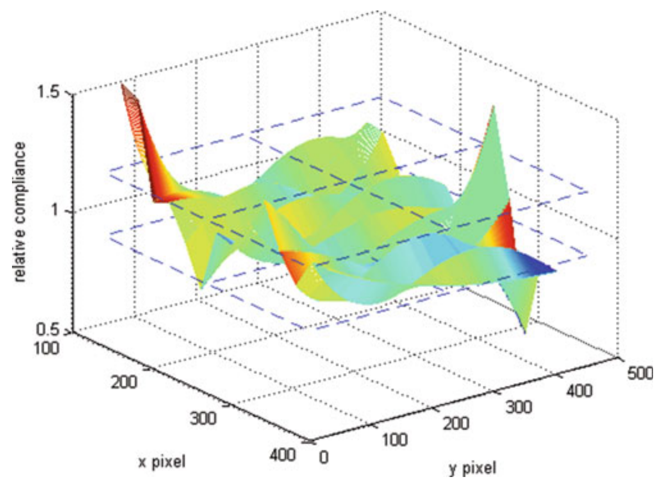

Fig. 15.8 Relative compliance (welded/non-welded)

relative compliance based on the acoustic velocity measurement, indicating the consistency of the ESPI measurement and acoustoelastic measurement.

Usually, the change in the elastic constant is ascribed to the non-linear elasticity of the inter-atomic potential. The nonlinearity is expressed via the third-order term of the potential [5, 6], where the first order term represents a reference potential and the second-order term the Young's modulus. The Young's modulus and the third order term of steel are typically 200 GPa and −500 GPa, respectively [6].

$$\frac{d\sigma}{d\varepsilon} = C^{(2)} + C^{(3)}\varepsilon = 200 - 500\varepsilon \tag{15.1}$$

Here σ is the stress, $C^{(2)}$ is the Young's modulus, $C^{(3)}$ is the third order term of the elastic constant and ε is the strain. The relative elastic constant (the reciprocal of the relative compliance) can be expressed as

$$\left(\frac{d\sigma}{d\varepsilon}\right)/\left(\frac{d\sigma}{d\varepsilon}\right)_0 = (200 - 500\,\varepsilon)/200 = 1 - \frac{5}{2}\varepsilon \tag{15.2}$$

If the observed change in the phase velocity of 6 % is due to the third order term of elastic constant, the value of Eq. (15.2) must be in the range of 1.06^2–0.94^2. From Eq. (15.2), the corresponding strain is −0.0494 (compressive) to 0.0464 (tensile). Since the yield strain of steel is typically 0.2 % = 0.002 or lower, these numbers are much higher to explain the observation by the nonlinear elasticity. Thus, the observed change in the compliance must be attributed to plastic deformation.

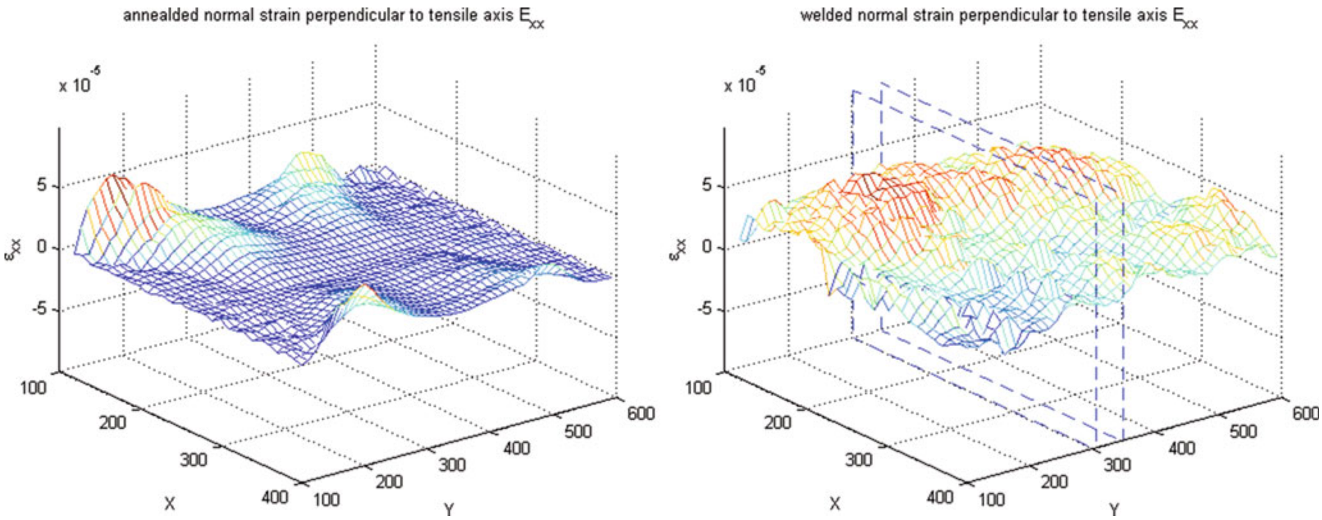

Fig. 15.9 Strain observed in non-welded (*left*) and welded (*right*) specimen 2

It should be noted that these strain values (−0.0494 and 0.0464) are two orders of magnitude higher than the corresponding value of the maximum residual stress measured with the strain gauge; 168.7 MPa/200 GPa = 8.4×10^{-4} (See Table 15.1. Here the residual strain is evaluated as the ratio of the measured residual stress 168.7 MPa to the Young's modulus 200 GPa). This is understandable because the strain gauge is sensitive only to the elastic portion of the residual strain while the acoustic wave velocity is determined by the overall elasticity of the region that can be partially plastically deformed.

Figure 15.9 shows strain plots for the non-welded and welded cases of specimen 2. For specimen 2, the ESPI setup was sensitive to both x (perpendicular to the tensile axis) and y (parallel to the tensile axis) components of the in-plane displacement. In this case, the effect of the welding is most prominent in the normal strain ε_{xx}. Like the case of specimen 1, the strain observed in the welded specimen shows vigorous fluctuations.

Figure 15.10 compares the y-dependence of ε_{xx} and ε_{yy} measured by the strain gauge and ε_{xx}, ε_{yy}, ε_{xy} (shear strain) and ω_z (rotation). Here dashed lines are the non-welded cases and solid lines are the welded cases. The strain gauge data show much higher correlation with shear and rotation than the normal strains. This supports the proposition that the effect of residual stress is not a simple superposition of the residual stress and the external stress but instead more overall response of the material.

The overall response of the specimen as a whole to the external load can be seen more clearly in Fig. 15.11 where contour plots of all strains and rotation are compared between the non-welded cases (left column) and the welded cases (right column). The normal strains (the first two rows from the top) indicate that the welding causes the deformation due to the tensile load to be less symmetric. Under tensile loading of a thin plate with no transverse constraint, the deformation is essentially symmetric. In a specimen of isotropic material with no initial stress concentration, the normal strain parallel to the tensile axis should be uniform, and the normal strain perpendicular to the tensile axis should be symmetric about the central line on the specimen parallel to the tensile axis. The top two contour plots on the left column certainly indicate these features for the non-welded case. [The ε_{yy} observed near the two horizontal ends (corresponding to the two ends gripped by the tensile machine) appears lower than the horizontal middle section. This is considered to be due to the lateral constraint by the tensile machine's grip.] On the other hand, the normal strains in the welded specimen do not show these feature. The ε_{xx} plot does not show the symmetry about the central line parallel to the tensile axis; instead, it exhibits some degree of symmetry about the diagonal line running from the top left corner to the bottom right corner of the specimen. The ε_{yy} plots does not indicate the uniform strain in the middle section but exhibits strain concentration near the bottom of the specimen about halfway to the right from the weld line. The contour plots of the shear strain and rotation are consistent with the above observations. The shear strain contours in the welded specimen shows a high value near the above-mentioned strain concentration. The rotation contours in the welded specimen exhibits much higher clockwise rotation in the middle section of the specimen. The displacement field plots shown in Fig. 15.12 are consistent with the observation. The displacement vectors of the welded case are similar to the non-welded case going from the right end through the middle of the right side of the weld. However, starting around this region toward the left end of the specimen, the displacement vectors of the welded specimen clearly indicate the tendency that the material rotates clockwise as a whole.

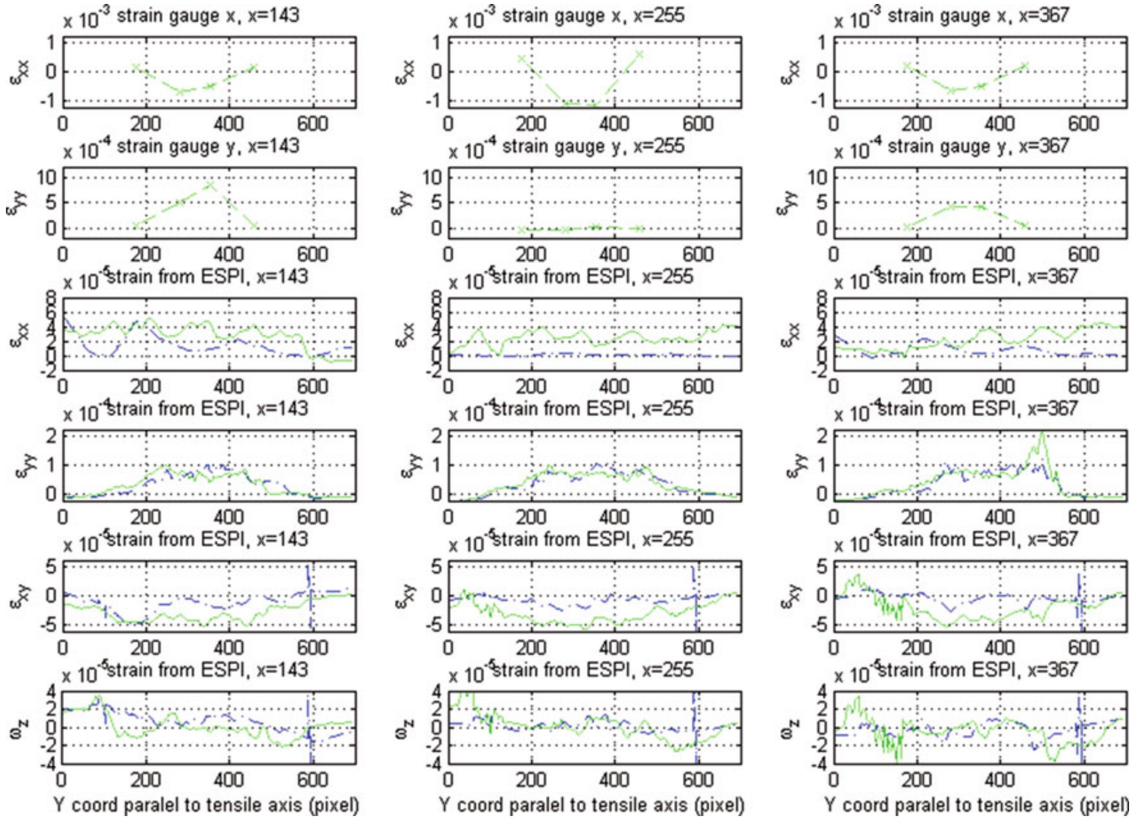

Fig. 15.10 Comparison of strain measured with the strain gauge and strain and rotation measured by ESPI

Fig. 15.11 Contour plots of strain and rotation

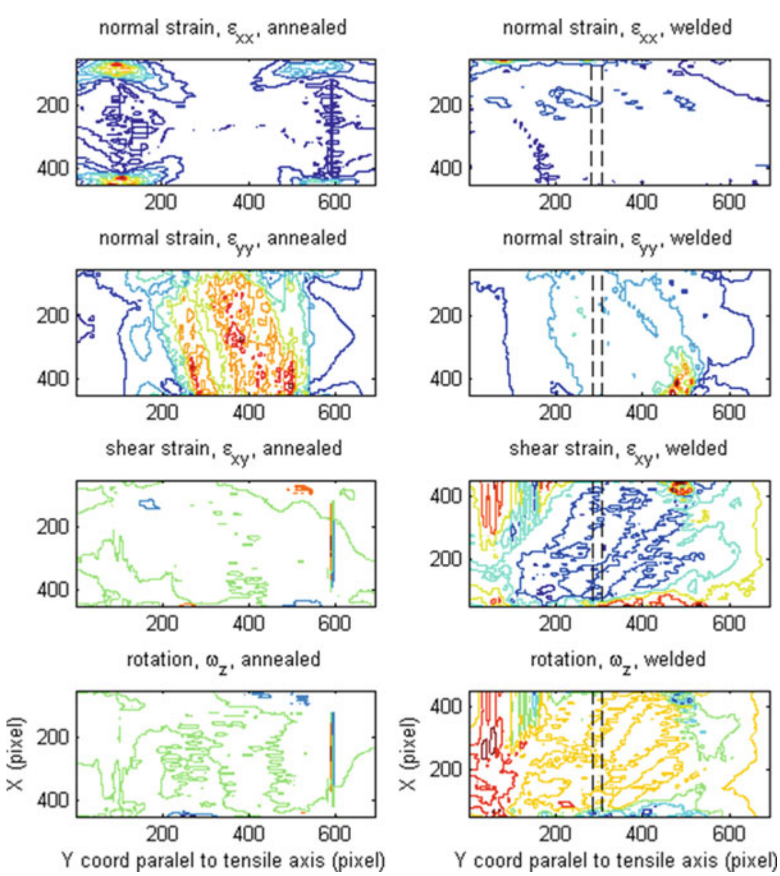

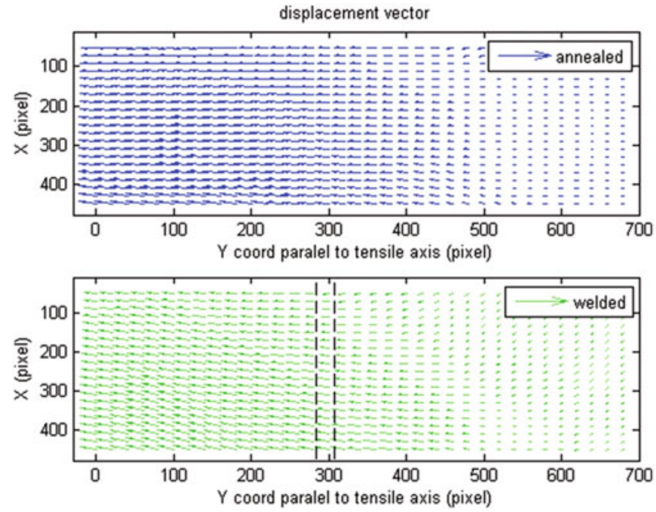

Fig. 15.12 Displacment vector field observed in the non-welded specimen (*top*) and in the welded specimen (*bottom*)

From the viewpoint of the residual stress, the above observations can be explained as follows. In Fig. 15.10, the strain gauge data indicates high compressive ε_{xx} near the weld ($y \approx 300$ pixel), and very low ε_{yy} near the weld around the vertical center (middle column). The high compressive ε_{xx} near the weld indicates that the stiffness parallel to the weld line is increased in this region. This hinders the specimen from experiencing the natural deformation, when the external load is applied, that the central portion contracts due to the Poisson's effect and the tensile deformation along the tensile axis is uniform. In accordance with the Poisson's effect, the material must somehow have compressive strain perpendicular to the tensile axis. The easiest location for the specimen to have compressive ε_{xx} strain is where the residual ε_{xx} turns the sign from negative (compressive) to positive (tensile). In the present case, this happens to be near $y \approx 200$ and $y \approx 420$ pixel (see top row of Fig. 15.10). Since between these two locations in y the material has difficulty in contraction, the stress is concentrated around $y \approx 200$ and $y \approx 420$ pixel. This explains the high shear strain between $y \approx 200$ and $y \approx 420$ pixel (third row, right column in Fig. 15.11 contour plots). Interestingly, the rotation changes the sign near $y \approx 100$ (bottom right plots in Fig. 15.10). The opposite rotations on the opposite sides of $y \approx 100$ indicate that the total angular momentum must remain zero, as the tensile machine does not exert torque. Note that the strain gauge and acoustic microscopic measurement indicate that the residual stress is substantially negligible at the point of the stress concentration.

15.4 Conclusions

In summary, this analysis indicates that the effect of residual stress due to welding is not necessarily limited near the weld where the residual stress itself is high. The change in the constitutive property of the material due to the residual stress alters the response of the material as a whole when an external load is applied. The findings resulting from this study can be summarized as follows:

1. The thermal load due to the welding has greater effect parallel to the weld than perpendicular as reported in ref 3.
2. The high compressive residual stress near the weld hinders natural compressive deformation due to the Poisson effect when an external tensile is applied.
3. The above effect can cause a stress concentration at a location some distance away from the weld where the residual stress is negligible.

Acknowledgment This work was supported by the National Research Foundation of Korea (NRF) grants funded by the Korean government MEST, NRF-2013R1A2A2A05005713, NRF-2013M2A2A9043274, and the National Science Foundation (IRES: 0927033).

References

1. Bate SK, Green D, Buttle D (1997) A review of residual stress distributions in welded joints for the defect assessment of offshore structures. Health and Safety Executive—offshore technology report
2. Colegrove P, Ikeagu C, Thistlethwaite A, Williams S, Nagy T, Suder W, Steuwer A, Pirling T (2009) The welding process impact on residual stress and distortion. Sci Technol Weld Join 14(8):717–725
3. Karlsson L (2005) Residual stresses due to welding of a nozzle to a pressure vessel. Master's dissertation, Division of Solid Mechanics, Lund University, Sweden
4. Every AG, Sachse W (1990) Determination of the elastic constants of anisotropic solids from acoustic-wave group-velocity measurements. Phys Rev B Condens Matter 42:8196–8205
5. Muir DD (2009) One-sided ultrasonic determination of third order elastic constants using angle-beam acoustoelasticity measurements. Ph.D. thesis, School of Electrical and Computer Engineering, Georgia Institute of Technology
6. Stobbe DM (2005) Acoustoelasticity in 7075-T651 aluminum and dependence of third order elastic constants on fatigue damage. Master's thesis, School of Electrical and Computer Engineering, Georgia Institute of Technology